Preprints.org

Article

On the Combination of the Laplace Transform and the Integral Equation Method to the 3D Parabolic Initial Boundary Value Problem

[Roman Chapko](#) * and [Sviatoslav Lavryk](#)

Article

On the Combination of the Laplace Transform and the Integral Equation Method to the 3D Parabolic Initial Boundary Value Problem

Roman Chapko [1],* , **Svyatoslav Lavryk** [1]

1   Department of Computational Mathematics, Ivan Franko National University of Lviv, Universytetska Str. 1, 79000 Lviv, Ukraine

*   Correspondence: roman.chapko@lnu.edu.ua

Abstract

We consider a two-step numerical approach for solving parabolic initial boundary value problems in the 3D simply connected smooth regions. The method uses the Laplace transform in time, reducing the problem to a set of independent stationary boundary value problems for the Helmholtz equation with complex parameters. The inverse Laplace transform is computed using sinc quadrature along a suitably chosen contour in the complex plane. We showed that due to a symmetry of the quadrature nodes, the number of stationary problems can be decreased by almost a factor of 2. The influence of the integration contour parameters on the approximation error is also researched. Stationary problems are numerically solved using boundary integral equation approach applying Nyström method, based on the quadratures for smooth surface integrals. Numerical experiments support the expectations.

Keywords: heat equation; Helmholtz equation; 3D initial boundary value problem; numerical Laplace transform inversion; boundary integral equation method; Nyström method; Wienert quadrature; sinc-quadratures

MSC: 35J05, 35K05, 35K20, 44A10, 45B05, 65D32, 65R10, 65R20

1. Introduction

The boundary integral equation (BIE) method is a very powerful approach for the numerical solution of various boundary value problems (BVPs). The main advantage of BIE method consists in the dimensionality decrease of the given differential problem: the BVP is reduced to the BIE, where the unknown function is defined only on the domain boundary [1]. Clearly, the considered differential equation needs to have the fundamental solution and to be homogeneous. For the numerical solution of such BIE, effective numerical methods are developed, for example, projection methods [1].

In the case of non-stationary BVPs, there are additional difficulties caused by the presence of time as an independent variable. There are several ways to apply BIE to such BVPs. One approach involves a fundamental solution of the time-dependent differential equation. Then, by a direct or indirect BIE method, the initial BVP can be reduced to a time-boundary integral equation. The numerical solution of such a BIE is more difficult than in the stationary case. The most popular method for time-boundary integral equations is the convolution quadrature method suggested by Christian Lubich in the 1980s [2].

Another so-called two-steps methods consist of the semi-discretization of the given initial BVP with respect to the time variable. As a result, the set of stationary BVPs for elliptic equations is obtained. This time discretization can be achieved using approaches such as finite-difference approximations (e.g., the Rothe method [3]) or integral transforms (e.g., the Laguerre transform [4–7], the Laplace

transform [8]). In the second step, which addresses the spatial variable, various techniques are available, including the BIE method. Two-step methods offer several advantages, such as dimension reduction and the avoidance of volume integrals. The finite-difference semi-discretization is the simplest approach, which gives the numerical solution in a fixed set of time moments. In the case of the integral transforms, we have an approximation for arbitrary time, but it is necessary to calculate the inverse transform numerically.

The Laguerre transform for a parabolic initial BVP leads to stationary BVPs for a recurrent sequence of elliptic equations, and to apply the BIE method, one needs to find the fundamental sequence [4,7]. The inverse Laguerre transform has the form of the Fourier-Laguerre series, and its summation is a complicated ill-posed problem, especially for long-time moments. In the case of the Laplace transform to a parabolic initial BVP, stationary BVPs for the Helmholtz-type equations with complex parameters can be obtained. The inverse Laplace transform is defined as the Bromwich integral on the complex plane, and there are several numerical methods for its calculation [9].

In this paper, we use the two-step approach based on the Laplace transform and the BIE method to solve parabolic BVPs in 3D domains. To calculate the inverse transform, the sinc-quadrature rule suggested in [10] is applied. Our contribution is to reduce computational costs by selecting optimal values of the quadrature formula parameters and applying an efficient method for numerically solving the resulting BIEs.

The outline of the present work is as follows. In Section 2, we apply the Laplace transform to the parabolic initial boundary value problem and describe the sinc-quadrature for the numerical inverse transform. Two ideas for decreasing computational cost are presented in subsections 2.1 and 2.2. In Subsection 2.1 it is shown that due to a certain symmetry of the sinc-quadrature nodes, the number of stationary problems can be reduced almost twice. In Subsection 2.2, it reflects how the choice of integration contour in the complex plane influences the precision of the sinc-quadrature. In Section 3, we apply the indirect BIE method to stationary elliptic problems. The unknown solution is presented in the form of the double-layer potential, and the BIE of the second kind is obtained. Taking into account that the boundary surface is diffeomorphic to the unit sphere we apply the Nyström method based on the Wienert's quadrature rules. Section 4 presents numerical examples to clarify our approach and its optimization.

Before closing this section, we formulate the problem to be studied. Let $D \subset \mathbb{R}^3$ be a simply connected region with a smooth boundary Γ. It is necessary to find function $u \in C^{2,1}(D \times (0,\infty)) \cap C(\overline{D} \times [0,\infty))$, which satisfies the heat equation

$$\frac{\partial u}{\partial t}(x,t) = \Delta u(x,t), \quad (x,t) \in D \times (0,\infty), \tag{1}$$

the initial condition

$$u(x,0) = 0, \quad x \in D \tag{2}$$

and the Dirichlet boundary value condition

$$u(x,t) = g(x,t), \quad (x,t) \in \Gamma \times (0,\infty). \tag{3}$$

Assume that the given function g is bounded, continuous, and satisfies the compatibility condition $g(x,0) = 0, \quad x \in \Gamma$.
We consider surfaces Γ, diffeomorphic to the unit sphere

$$\mathbb{S}^2 = \{p(\theta,\phi) = (\sin\theta\cos\phi, \sin\theta\sin\phi, \cos\theta), (\theta,\phi) \in [0,\pi] \times [0,2\pi]\}$$

described by an analytic function $q : \mathbb{S}^2 \to \Gamma$ with a non zero Jacobian J.

2. Time Semi-Discretization via Laplace Transform

The Laplace transform of the function $f(t)$ is given by

$$\mathcal{L}_t(f) = F(s) = \int_0^\infty e^{-st} f(t) dt, \quad s = \sigma + i\tau, \; s \in \mathbb{C}. \tag{4}$$

The integral (4) is convergent for $\mathrm{Re}(s) > a_0$, where a_0 is the order of growth of the function $f(t)$, and $F(s)$ is an analytic function.

For the known image F the original f can be reconstructed by using the inverse Laplace transform, described by the Bromwich integral

$$\mathcal{L}_s^{-1}(F) = f(t) = \frac{1}{2\pi i} \int_C e^{st} F(s) ds, \tag{5}$$

where C is the suitable integration contour (see [8], [10], [11]).

A popular strategy to use the Laplace transform for the heat problems is next:

1. Apply the Laplace transform in time to the initial boundary value problem to obtain boundary value problems for the Helmholtz-type equations.
2. Build an effective solver for stationary problems.
3. Reconstruct time-domain solution via numerical inversion of the Laplace transform.

One approach to approximating the inverse Laplace transform was proposed in [10]. If F can be analytically continued to the set $\mathbb{C} \setminus \Sigma_\delta$, where

$$\Sigma_\delta = \left\{ s \in \mathbb{C} : |\arg(-s)| \leq \delta, \quad 0 < \delta < \frac{\pi}{2} \right\}$$

and there exists $M > 0$ such that

$$|F(s)| \leq \frac{M}{|s|}, \quad s \in \mathbb{C} \setminus \Sigma_\delta,$$

then to approximate the inverse Laplace transform of the function F, a quadrature formula is proposed based on the use of sinc-quadrature for integral (5) with a special integration contour (see Figure 1)

$$\gamma(\omega) = \lambda\big(1 - \sin(\alpha + i\omega)\big), \quad \omega \in \mathbb{R}. \tag{6}$$

Here $\lambda > 0, 0 < \alpha < \frac{\pi}{2} - \delta$ are arbitrary parameters that define the geometry of the contour (6).
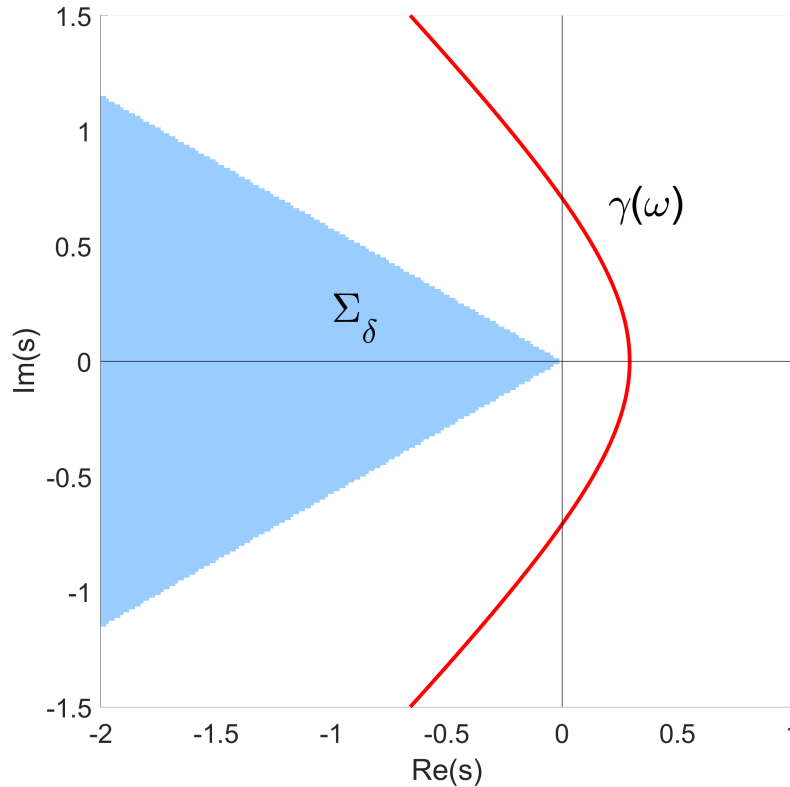
Figure 1. Set Σ_δ and integration contour $\gamma(\omega)$, $\delta = \pi/6$, $\alpha = \pi/4$, $\lambda = 1$

Using contour (6) to parametrize integral (5), we obtain

$$\mathcal{L}_s^{-1}(F) = f(t) = -\frac{1}{2\pi i} \int_{-\infty}^{\infty} e^{\gamma(\omega)t} F(\gamma(\omega)) \gamma'(\omega) d\omega. \tag{7}$$

Let $N_t > 0$, $N_t \in \mathbb{N}$, $h_N = \ln N_t / N_t$, $\omega_j = h_N j$, $j = -N_t, ..., N_t$. Integral (7) can be approximated using the following quadrature formula [10]

$$f(t) \approx (T_{N_t} F)(t) = \frac{h_N}{2\pi i} \sum_{j=-N_t}^{N_t} e^{\gamma(\omega_j)t} F(\gamma(\omega_j)) \gamma'(\omega_j). \tag{8}$$

Let us denote $s_j = \gamma(\omega_j)$ and $\gamma_j = h_N \gamma'(\omega_j)/2\pi i$, then we obtain

$$f(t) \approx (T_{N_t} F)(t) = \sum_{j=-N_t}^{N_t} \gamma_j e^{ts_j} F(s_j). \tag{9}$$

Note, when computing $(T_{N_t} F)(t)$ for different values of t, one can use the same set of values $F(s_j)$. The approximation error of (9) is shown to behave like $\mathcal{O}\left(e^{-cN_t / \ln N_t}\right)$ and possess stability to the perturbations of $F(s_j)$. This is especially important when values $F(s_j)$ are computed numerically [10].

Since the solution of the non-stationary problem (1)–(3) u is bounded with respect to the time variable, i.e., its order of growth is equal to 0, the Laplace transform with respect to time can be applied to both parts of equation (1). Taking into account property $\mathcal{L}_t(f'(t)) = sF(s) - f(0)$ and zero initial condition, we obtain the following equation for the Laplace image $U_s(x) = \mathcal{L}_t(u(x,t))$

$$\Delta U_s(x) - sU_s(x) = 0, \quad x \in D. \tag{10}$$

On the boundary of the domain, the function U_s satisfies the following condition

$$U_s(x) = G_s(x), \quad x \in \Gamma, \tag{11}$$

where $G_s(x) = \mathcal{L}_t(g(x,t))$. Thus, for U_s we get a boundary value problem (10)–(11) for the Helmholtz equation with a complex wavenumber $\kappa^2 = -s$.

Applying the described approach for the inverse Laplace transform, in order to find an approximate solution of problem (1)–(3), it is necessary to compute

$$U_j(x) = U_{s_j}(x), \ j = -N_t, ..., N_t,$$

that is, to solve a set of $2N_t + 1$ problems (10)–(11) for $s = s_j$

$$\Delta U_j(x) - s_j U_j(x) = 0, \quad x \in D, \tag{12}$$

$$U_j(x) = G_j(x), \quad x \in \Gamma. \tag{13}$$

Here $G_j(x) = G_{s_j}(x)$. It is important to emphasize that problems (12)–(13) are independent of each other, enabling their parallel solution.

In [8], [11] it was shown that the image of the solution to the heat problem U_s, as a function of the complex argument s, can be analytically continued to the set $Z = \mathbb{C} \setminus (-\infty, 0]$, and there exists a constant $M > 0$ such that

$$|U_s(\cdot)| \le \frac{M}{|s|}, \quad s \in Z.$$

Thus, in our case, we can apply the approach from [10] and use the contour (6) for any $\lambda > 0$ and $0 < \alpha < \frac{\pi}{2}$.

Note, in order to solve problems (12)–(13) it is necessary to have boundary functions G_j, i.e., have the Laplace image G_s of the original boundary condition g. If G_s is not available in a closed form, it can be approximated using various techniques (see [12],[13],[14]). We leave the approximation of G_s beyond the scope of the current article and will use examples of g with a known Laplace transform for the numerical experiments.

Recalling problems (12)–(13) are 3D stationary boundary value problems, it is easy to see that solving them numerically may pose a significant computational effort. The main motivation for this article was to suggest certain ideas for decreasing the amount of computational work, as described further.

2.1. Reducing Number of Stationary Problems

It is easy to notice that $\omega_{-j} = -\omega_j, j = 1, ..., N_t$.

Then

$$s_{-j} = \gamma(\omega_j) = \lambda\left(1 - \sin(\alpha + i\omega_j)\right) =$$

$$= \lambda\left(1 - \sin(\alpha - i\omega_{N_t - j})\right) = \overline{\lambda\left(1 - \sin(\alpha + i\omega_{N_t - j})\right)} = \overline{s_j}, \quad j = 1, ..., N_t. \tag{14}$$

We use the fact that $\overline{\sin(z)} = \sin(\overline{z})$ for any complex z.

Thus, quadrature nodes (14) are pairwise conjugate, except for the node s_0. This allows reducing the solution of the set of $2N_t + 1$ stationary problems to $N_t + 1$ problems.

We show that

$$U_{-j}(x) = \overline{U_j(x)}, \quad j = 1, ..., N_t.$$

Theorem 1. *Let U be a solution of the problem*

$$\Delta U(x) - sU(x) = 0, \quad x \in D, \tag{a}$$

$$U(x) = G(x), \quad x \in \Gamma. \tag{b}$$

Then $\overline{U}$ is a solution of the problem

$$\Delta\overline{U(x)} - \overline{s}\,\overline{U(x)} = 0, \quad x \in D, \tag{c}$$

$$\overline{U(x)} = \overline{G(x)}, \quad x \in \Gamma. \tag{d}$$

Proof. Statement (d) follows directly from (b). Let us show that (c) follows from (a). We denote

$$s = a + ib, \quad U(x) = V(x) + iW(x),$$

$$\overline{s} = a - ib, \quad \overline{U(x)} = V(x) - iW(x).$$

Then (a) can be written as

$$\Delta V(x) + i\Delta W(x) = aV(x) - bW(x) + i(bV(x) + aW(x))$$

Thus

$$\Delta V(x) = aV(x) - bW(x), \ \Delta W(x) = bV(x) + aW(x).$$

Then

$$\Delta\overline{U(x)} = \Delta V(x) - i\Delta W(x) =$$

$$= aV(x) - bW(x) - ibV(x) - iaW(x) =$$

$$= (a - ib)V(x) - i(a - ib)W(x) =$$

$$= (a - ib)(V(x) - iW(x)) = \overline{s}\,\overline{U(x)},$$

which proves statement (c). □

Corollary 1. *Solutions of the problems* (12) - (13) *with indices* $-j$ *and* j *are complex conjugates*

$$U_{-j}(x) = \overline{U_j(x)}, \quad j = 1, \ldots, N_t.$$

Proof. Using a well-known fact $F(\overline{s}) = \overline{F(s)}$ (for real valued $f(t)$) it is easy to see that the boundary conditions of the problems with indices $-j$ and j are complex conjugates. Since $s_{-j} = \overline{s_j}$, it follows from the Theorem 1 the solutions of the problems (12) - (13) with indices $-j$ and j are also complex conjugates. □

Thus, it is sufficient to solve the stationary problems for indices $j = 0, \ldots, N_t$, and the solutions for the indices $j = -N_t, \ldots, -1$ can be obtained automatically from the Corollary 1.

2.2. Integration Contour Parameters Optimization

As mentioned earlier, the integration contour (6) depends on the parameters $\lambda > 0$ and $0 < \alpha < \frac{\pi}{2}$. The Figures 2 and 3 show the influence of the parameters α and λ on the shape of the contour and placement of the nodes for $N_t = 4$
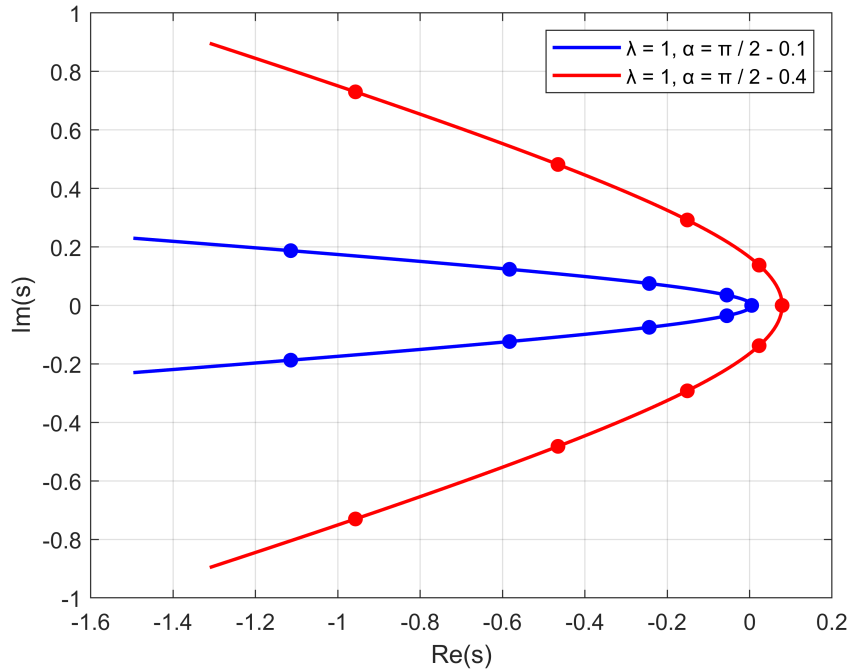
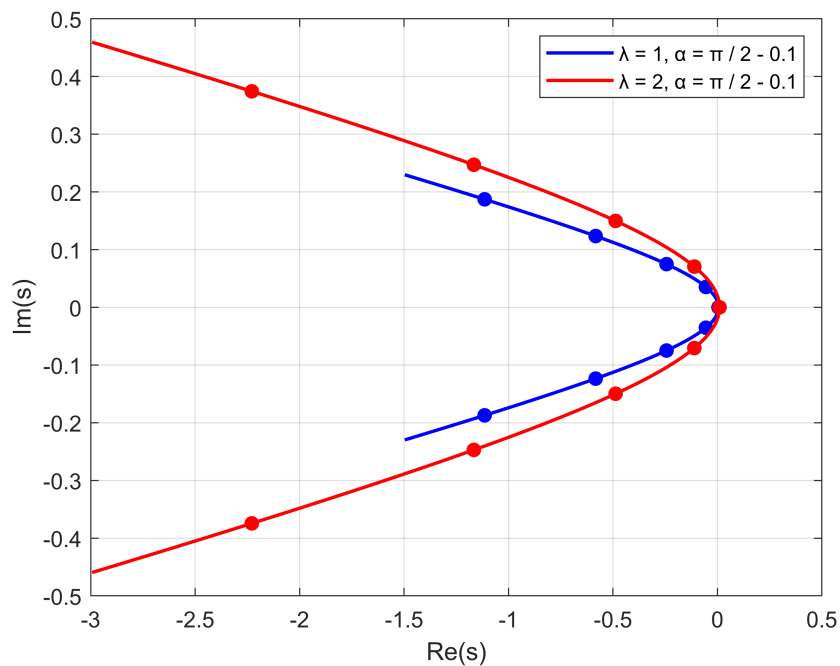**Figure 2.** Influence of α on the integration contour

Figure 3. Influence of λ on the integration contour

Since the approximate solution of the 3D stationary problems requires a large amount of computations, it makes sense to select the parameters α, λ in such a way as to reduce the expected error.

To find the parameters α, λ for which the error is minimized, we will define search intervals for the optimal values of α, λ and construct a uniform grid of test values for α, λ

$$\alpha \in [\alpha_0, \alpha_1] \subset (0; \pi/2), \quad \lambda \in [\lambda_0, \lambda_1] \subset (0; \infty),$$

$$\alpha_\nu = \alpha_0 + \nu h_\alpha, \quad \nu = 0, ..., N_\alpha, N_\alpha \in \mathbb{N}, \quad h_\alpha = (\alpha_1 - \alpha_0)/N_\alpha, \tag{15}$$

$$\lambda_\mu = \lambda_0 + \mu h_\lambda, \quad \mu = 0, ..., N_\lambda, N_\lambda \in \mathbb{N}, \quad h_\lambda = (\lambda_1 - \lambda_0)/N_\lambda. \tag{16}$$

We fix certain values of x, t, N_t and select a Laplace transform pair of test functions $u^T(x,t)$ and $U^T(x,s)$. It is natural to select u^T to be similar to the behavior of the boundary condition g. Then, for each pair of values $(\alpha_\nu, \lambda_\mu)$, we compute the absolute or relative errors E_{abs}, E_{rel} of the numerical Laplace transform inversion (9) for $U^T(x,s)$ and find the values $(\alpha_{\min}, \lambda_{\min})$ for which

$$E_{abs,min} = min\{E_{abs} \mid (\alpha_{\nu,\lambda_\mu}), \nu = 0, ..., N_\alpha, \mu = 0, ..., N_\lambda\}, \tag{17}$$

$$E_{rel,min} = min\{E_{rel} \mid (\alpha_{\nu,\lambda_\mu}), \nu = 0, ..., N_\alpha, \mu = 0, ..., N_\lambda\}. \tag{18}$$

Obtained contour parameters $(\alpha_{\min}, \lambda_{\min})$ are then used to define quadrature nodes s_j and solve $N_t + 1$ stationary problems. We do not provide an explicit recipe to define $[\alpha_0, \alpha_1]$ and $[\lambda_0, \lambda_1]$. For $[\alpha_0, \alpha_1]$ it seems natural to define α_0 close to 0 and α_1 close to $\pi/2$ and thus "scan" most of the $(0; \pi/2)$ interval. For $[\lambda_0, \lambda_1]$ it is empirically observed that increasing λ_1 stops finding different λ_{min} after certain values of λ_1.

3. Stationary Boundary Value Problems Solver

In this section we consider the numerical solution of the stationary problems (12)–(13). We will apply the BIE method with later application of the Nyström method based on the quadrature rules for surface integrals, proposed by Wienert [15].
For brevity, we rewrite problems (12)–(13) as

$$\Delta U_s(x) - sU_s(x) = 0, \quad x \in D, \; s \in \{s_j, \; j = 0, ..., N_t\}, \tag{19}$$

$$U_s(x) = G_s(x), \quad x \in \Gamma. \tag{20}$$

The fundamental solution of the equation (19) has the form

$$\Phi_s(x,y) = \frac{1}{4\pi} \frac{e^{-k|x-y|}}{|x-y|}, \quad x, y \in \mathbb{R}^3, \; x \neq y, \tag{21}$$

$$k = \sqrt{s}, \quad Re(\kappa) > 0.$$

Since $s \notin (-\infty, 0]$, it is known that under suitable assumptions on the boundary Γ and for sufficiently smooth boundary data G_s, the solution of the Dirichlet problem exists and is unique, see [16] and references therein. The solution of (19) can be written in the form of a double layer potential

$$U_s(x) = \int_\Gamma \varphi(y) \Phi_{\nu,s}(x,y) ds(y), \quad x \in \Gamma, \tag{22}$$

where $\Phi_{\nu,s}(x,y) = \frac{\partial \Phi_s(x,y)}{\partial \nu(y)}$, $\varphi(y)$ is the potential density and $\nu(y)$ is the unit outward normal vector to Γ at the point y.

Potential (22) is a solution of the problem (12)–(13) if the density φ is a solution of the Fredholm integral equation of the second kind

$$-\frac{1}{2}\varphi(x) + \int_\Gamma \varphi(y) \Phi_{\nu,s}(x,y) ds(y) = G_s(x), \quad x \in \Gamma. \tag{23}$$

For any $G_s \in C(\Gamma)$ equation (23) has a unique solution φ in $C(\Gamma)$ [16].
Since $\Gamma = \{x = q(\hat{x}), \hat{x} \in \mathbb{S}^2\}$, we can obtain the parametrized integral equation on $\mathbb{S}^2$

$$-\frac{1}{2}\psi(\hat{x}) + \int_{\mathbb{S}^2} \psi(\hat{y}) K(\hat{x}, \hat{y}) ds(\hat{y}) = \hat{G}_s(\hat{x}), \quad \hat{x} \in \mathbb{S}^2, \tag{24}$$

where we denoted $\psi(\hat{x}) = \varphi(q(\hat{x}))$, $\hat{G}_s(\hat{x}) = G_s(q(\hat{x}))$, $\hat{x} \in \mathbb{S}^2$ and

$$K(\hat{x}, \hat{y}) = \Phi_{\nu,s}(q(\hat{x}), q(\hat{y}))J(\hat{y}), \quad \hat{x}, \hat{y} \in \mathbb{S}^2, \, \hat{x} \neq \hat{y}.$$

The function K is a weakly singular integral kernel that can be rewritten in the form

$$K(\hat{x}, \hat{y}) = \frac{M(\hat{x}, \hat{y})}{|\hat{x} - \hat{y}|}, \quad \hat{x}, \hat{y} \in \mathbb{S}^2, \, \hat{x} \neq \hat{y},$$

where

$$M(\hat{x}, \hat{y}) = \frac{e^{-k|q(\hat{x}) - q(\hat{y})|}}{4\pi} \frac{(q(\hat{x}) - q(\hat{y}), \nu(q(\hat{y})))}{|q(\hat{x}) - q(\hat{y})|^2} \frac{|\hat{x} - \hat{y}|J(\hat{y})}{|q(\hat{x}) - q(\hat{y})|} (k|q(\hat{x}) - q(\hat{y})| + 1).$$

Note, due to the analyticity of q well-posedness of (23) also applies to (24). In order to discretize (24), we consider quadrature rules, proposed by Wienert [15]. For a given space discretization parameter $N \in \mathbb{N}$ the following values are defined

$$\hat{p}_{\beta,\mu} = p(\vartheta_\beta, \varphi_\mu), \vartheta_\beta = \arccos \xi_\beta, \, \varphi_\mu = \frac{\pi}{N}\mu, \tag{25}$$

$$w_\beta^{(1)} = \frac{2\pi}{N(1 - \xi_\beta^2)(P_N'(\xi_\beta))^2}, \quad \beta = 1, \ldots, N, \, \mu = 0, \ldots, 2N - 1.$$

where $\xi_1 < \cdots < \xi_N$ are the zeros of the Legendre polynomials P_N [17].
For a given function $f \in C(\mathbb{S}^2 \setminus \{(0, 0, \pm 1)\})$ approximation $A_N f$ is defined as

$$(A_N f)(\hat{x}) = \sum_{\beta=1}^{N} \sum_{\mu=0}^{2N-1} w_\beta^{(1)} f(\hat{p}_{\beta,\mu}) \, a_{\beta,\mu}(\hat{x}), \tag{26}$$

where $a_{\beta,\mu}(\hat{x}) = \sum_{n=0}^{N-1} \frac{2n+1}{4\pi} P_n(\hat{x} \cdot \hat{p}_{\beta,\mu})$ and by $\hat{x} \cdot \hat{p}_{\beta,\mu}$ we denote a scalar product of two vectors. Note, the poles are excluded from the continuity requirements, since values of the parametrized functions $f \circ p$ at the poles may depend on the direction of approach (i.e. specific value of φ) and may be not continous at the poles.
For the non-singular integrands, the following quadrature rule is suggested

$$\int_{\mathbb{S}^2} f(\hat{y}) \, ds(\hat{y}) \approx \int_{\mathbb{S}^2} (A_N f)(\hat{y}) \, ds(\hat{y}) = \sum_{\beta=1}^{N} \sum_{\mu=0}^{2N-1} w_\beta^{(1)} f(\hat{p}_{\beta,\mu}). \tag{27}$$

For the weakly singular integrands, the following quadrature rule can be used

$$\int_{\mathbb{S}^2} \frac{f(\hat{y})}{|\hat{n}_p - \hat{y}|} \, ds(\hat{y}) \approx \int_{\mathbb{S}^2} \frac{(A_N f)(\hat{y})}{|\hat{n}_p - \hat{y}|} \, ds(\hat{y}) = \sum_{\beta=1}^{N} \sum_{\mu=0}^{2N-1} w_\beta^{(2)} f(\hat{p}_{\beta,\mu}), \tag{28}$$

where $w_\beta^{(2)} = w_\beta^{(1)} \sum_{n=0}^{N-1} P_n(\xi_\beta)$ and $\hat{n}_p = (0, 0, 1)$.

Both quadratures are obtained by approximation of the regular part of the integrand via approximation A_N and then using exact integration. According to results in [15], these quadrature rules have super-algebraic or even exponential convergence order, depending on the smoothness of f.

By simple substitution, the quadrature rule (28) can be extended to a more general case

$$\int_{\mathbb{S}^2} \frac{f(\hat{y})}{|\hat{x} - \hat{y}|} \, ds(\hat{y}) = \int_{\mathbb{S}^2} \frac{f(T_{\hat{x}}^{-1}\hat{y})}{|\hat{n}_p - \hat{y}|} \, ds(\hat{y}) \approx \sum_{\beta=1}^{N} \sum_{\mu=0}^{2N-1} w_\beta^{(2)} f(T_{\hat{x}}^{-1}\hat{p}_{\beta,\mu}), \, \hat{x} \in \mathbb{S}^2, \tag{29}$$

where $T_{\hat{x}}$ is usually a rotation, such that $T_{\hat{x}}\hat{x} = \hat{n}_p$, see [15].

Applying (29) to the integral in (24), for $\tilde{\psi} \approx \psi$ we get an approximation equation

$$-\frac{1}{2}\tilde{\psi}(\hat{x}) + \sum_{\beta=1}^{N}\sum_{\mu=0}^{2N-1} w_{\beta}^{(2)}\tilde{\psi}(T_{\hat{x}}^{-1}\hat{p}_{\beta,\mu})\, M(\hat{x}, T_{\hat{x}}^{-1}\hat{p}_{\beta,\mu}) = \hat{G}_s(\hat{x}), \quad \hat{x} \in \mathbb{S}^2. \tag{30}$$

We observe that (30) contains values of the density $\tilde{\psi}$ in the rotated nodes $T_{\hat{x}}^{-1}\hat{p}_{\beta,\mu}$. In order to be able to construct a system of linear equations, we replace $\tilde{\psi}(T_{\hat{x}}^{-1}\hat{p}_{\beta,\mu})$ with its approximation by A_N (26)

$$\tilde{\psi}(T_{\hat{x}}^{-1}\hat{p}_{\beta,\mu}) \approx (A_N\tilde{\psi})(T_{\hat{x}}^{-1}\hat{p}_{\beta,\mu}) = \sum_{\beta'=1}^{N}\sum_{\mu'=0}^{2N-1} w_{\beta'}^{(1)}\tilde{\psi}(\hat{p}_{\beta',\mu'})a_{\beta',\mu'}(T_{\hat{x}}^{-1}\hat{p}_{\beta,\mu}). \tag{31}$$

Substituting (31) back into (30), we get

$$-\frac{1}{2}\tilde{\psi}(\hat{x}) + \sum_{\beta'=1}^{N}\sum_{\mu'=0}^{2N-1} \tilde{\psi}(\hat{p}_{\beta',\mu'})w_{\beta',\mu'}^{(3)}(\hat{x}) = \hat{G}_s(\hat{x}), \quad \hat{x} \in \mathbb{S}^2, \tag{32}$$

where $w_{\beta',\mu'}^{(3)}(\hat{x}) = w_{\beta'}^{(1)} \sum_{\beta=1}^{N}\sum_{\mu=0}^{2N-1} w_{\beta}^{(2)} M(\hat{x}, T_{\hat{x}}^{-1}\hat{p}_{\beta,\mu})a_{\beta',\mu'}(T_{\hat{x}}^{-1}\hat{p}_{\beta,\mu})$.

Collocating the equation (32) in the nodes $\hat{p}_{\beta_2,\mu_2}$, $\beta_2 = 1,\ldots,N$, $\mu_2 = 0,\ldots,2N-1$, we get a $2N^2 \times 2N^2$ system of linear equations for the unknown values $\tilde{\psi}(\hat{p}_{\beta_2,\mu_2})$

$$-\frac{1}{2}\tilde{\psi}(\hat{p}_{\beta_2,\mu_2}) + \sum_{\beta'=1}^{N}\sum_{\mu'=0}^{2N-1} \tilde{\psi}(\hat{p}_{\beta',\mu'})w_{\beta',\mu'}^{(3)}(\hat{p}_{\beta_2,\mu_2}) = \hat{G}_s(\hat{p}_{\beta_2,\mu_2}). \tag{33}$$

After solving (33), the approximate solutions of problems (19)–(20) for the parameter $s = \{s_j, j = 0,\ldots,N_t\}$ can be found by applying the quadrature rule (27) to (22)

$$U_{j,N}(x) = \sum_{\beta_2=1}^{N}\sum_{\mu_2=0}^{2N-1} w_{\beta_2}^{(1)}\tilde{\psi}_j(\hat{p}_{\beta_2,\mu_2})\Phi_{\nu,s_j}(x, q(\hat{p}_{\beta_2,\mu_2}))J(\hat{p}_{\beta_2,\mu_2}), \quad x \in D, \; j = 0,\ldots,N_t, \tag{34}$$

where $\tilde{\psi}_j(\hat{p}_{\beta_2,\mu_2}) = \tilde{\psi}(\hat{p}_{\beta_2,\mu_2})$ for the parameter value $s = s_j$.

Having solved a set of problems (19)–(20), we can construct the approximate solution of the original non-stationary problem (1)–(3)

$$u(x,t) \approx u_{N_t,N}(x,t) = \sum_{j=0}^{N_t} \gamma_j e^{ts_j}U_{j,N}(x) + \sum_{j=-N_t}^{-1} \gamma_j e^{ts_j}\overline{U_{-j,N}(x)}. \tag{35}$$

As mentioned, the error rate of the numerical inversion of the Laplace transform behaves like $\mathcal{O}\left(e^{-cN_t/\ln N_t}\right)$ and is stable to perturbations of U_j values. In our case these perturbations are created by the fact that U_j are approximated by $U_{j,N}$, which in practice exhibits super-algebraic convergence rate for the sufficiently smooth surfaces and boundary conditions. As result, when N_t and N are selected in the balanced way, the overall error rate of the original non-stationary problem is super-algebraic, which is shown by the numerical experiments.

4. Numerical Experiments

We will consider the following examples of the regions D_k, $k = 1, 2$ and their boundaries Γ_k to perform numerical experiments (see Figure 4)

$$\Gamma_1 = \{r_1(\theta,\varphi)(\sin\theta\cos\phi,\, \sin\theta\sin\phi,\, \cos\theta),\, (\theta,\phi) \in [0,\pi] \times [0,2\pi]\},$$

$$r_1(\theta, \varphi) = A_1\left(0.6 + \sqrt{4.25 + 2\cos 3\theta}\right), \ A_1 \in \mathbb{R} > 0,$$

$$\Gamma_2 = \{r_2(\theta, \varphi)(\sin\theta\cos\phi, \sin\theta\sin\phi, \cos\theta), \ (\theta, \phi) \in [0, \pi] \times [0, 2\pi)\},$$

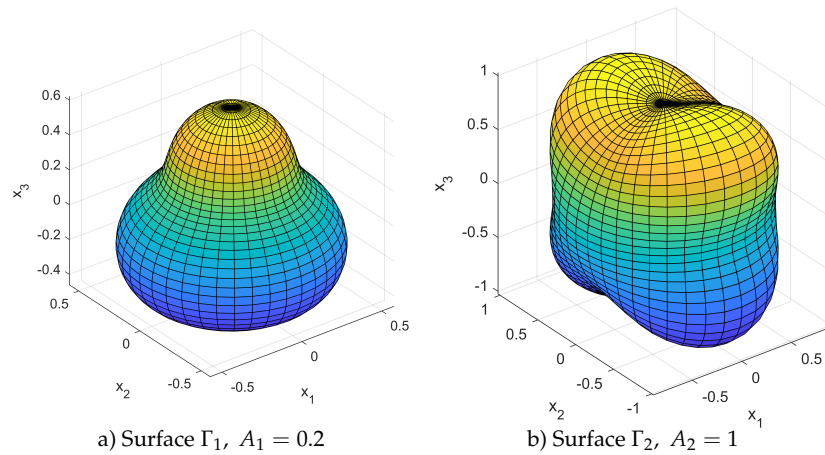$$r_2(\theta, \varphi) = A_2\sqrt{0.8 + 0.2(\cos(2\varphi) - 1)(\cos(4\theta) - 1)}, \ A_2 \in \mathbb{R} > 0.$$

a) Surface Γ_1, $A_1 = 0.2$ b) Surface Γ_2, $A_2 = 1$

Figure 4. Boundary surfaces.

Note, when defining specific surfaces Γ using mapping $q : \mathbb{S}^2 \to \Gamma$, it is possible to use spherical or Cartesian coordinates to describe points on the unit sphere. For the mentioned surfaces Γ_1 and Γ_2 we used spherical coordinates.

4.1. Inverse Laplace Transform

Here we test the numerical inversion of the Laplace transform and suggested optimizations. Let us consider the fundamental solution of the heat equation (1)

$$\tilde{G}(x, y, t) = \frac{1}{\sqrt{4\pi t^3}} e^{\frac{|x-y|^2}{4t}}, \quad x, y \in R^3, \ x \neq y, \ t > 0,$$

for which the Laplace image is a fundamental solution of the Helmholtz equation (10)

$$\mathcal{L}_t(\tilde{G}(x, y, t)) = \int_0^\infty e^{-st}\tilde{G}(x, y, t)dt = \Phi_s(x, y),$$

$$\mathcal{L}_s^{-1}(\Phi_s(x, y)) = \tilde{G}(x, y, t). \tag{36}$$

For a given source point $y^* \notin D_1$, function

$$w(x, t) = \tilde{G}(x, y^*, t), \ x \in D_1, \ y^* \notin D_1,$$

is an exact solution of the heat equation (1) and its Laplace transform $W_s(x) = \Phi_s(x, y^*)$ is an exact solution of the Hemholtz equation (10). Clearly, the Theorem 1 holds true in this case, so the values of W_s can be computed only at the nodes s_j, $j = 0, ..., N_t$.

To test the effect of the α, λ selection, we choose some random values of α_0, λ_0 and compare the absolute error $E_{abs} = |T_{N_t}(W_s) - w|$ for the approximate computation of the inverse Laplace transform (36) to the absolute error $E_{abs,min}$ for the optimal parameters $\alpha_{min}, \lambda_{min}$, obtained via optimization process (17).

Tables 1 and 2 show the comparison of $E_{abs,min}$ and E_{abs} for the different values of x, y^*, t.

Table 1. Errors $E_{abs,min}$ and E_{abs} for $x = (0.1, 0.1, 0.2)$, $y^* = (0,0,5)$, $t = 2$, $N_\alpha = 20$, $N_\lambda = 40$.

N_t	$E_{abs,min}$	α_{min}	λ_{min}	E_{abs}	α_0	λ_0
2	1.27e-08	0.989450	9.794872	2.88e-04	$\pi/2$ - 0.2	1
4	2.71e-11	0.826209	5.712821	2.00e-05	$\pi/2$ - 0.2	1
8	1.01e-15	1.071071	3.671795	5.56e-07	$\pi/2$ - 0.2	1
16	5.45e-20	1.071071	5.712821	8.75e-11	$\pi/2$ - 0.2	1

Table 2. Errors $E_{abs,min}$ and E_{abs} for $x = (0.1, 0.05, 0.05)$, $y^* = (0,0,4)$, $t = 1.5$, $N_\alpha = 30$, $N_\lambda = 60$.

N_t	$E_{abs,min}$	α_{min}	λ_{min}	E_{abs}	α_0	λ_0
2	6.44e-08	1.212716	8.869492	2.98e-04	$\pi/2$ - 0.2	1
4	1.16e-08	1.096689	4.822034	1.82e-04	$\pi/2$ - 0.2	1
8	3.11e-15	1.058013	6.171186	3.83e-06	$\pi/2$ - 0.2	1
16	1.04e-19	1.077351	9.206780	5.59e-09	$\pi/2$ - 0.2	1

Obtained results support expected error rates. Note, the tested $(\alpha_{min}, \lambda_{min})$ search routine is computationally fast (involves $N_\alpha \times N_\lambda$ Laplace inversions) and is negligible compared to the computational effort of solving the stationary 3D problem. Comparing specific values in tables 1 and 2 one could expect significant reduction in necessary N_t, i.e. number of stationary problems to solve.

4.2. Stationary Problem

In this section we test the numerical solution of the stationary problems (10)–(11) using BIE method, described in section 3. As a sample boundary condition we choose G_s as the narrowing of the fundamental solution $\Phi_s(\cdot, y^*)$ onto Γ with a source point y^* outside the region D_k. In this case the exact solution of the problem (10)–(11) is

$$U_s^*(x) = \Phi_s(x, y^*), \quad x \in D_k, \ y^* \notin D_k, \ k = 1, 2.$$

Let $y^* = (0,0,5) \notin D_k$, $k = 1, 2$. To measure the accuracy of the numerical approximation, we use the following discrete L_2 error

$$E_{L_2} = \frac{1}{\tilde{N}} \left(\sum_{m=1}^{\tilde{N}} \sum_{j=1}^{\tilde{N}} \left| U_{s_k}^*(x_{m,j}) - U_{k,N}(x_{m,j}) \right|^2 \right)^{1/2},$$

where $U_{k,N}$ is the approximate solution obtained by (34) and $\tilde{N} = 10$. The test points $x_{m,j}$ are uniformly distributed on a diminished artificial surface located within the solution domain, according to the following rule

$$x_{m,j} = 0.5 r_k(\theta_m, \phi_j) p(\theta_m, \phi_j), \ \theta_m = \frac{\pi}{\tilde{N}+1} m, \ \phi_j = \frac{2\pi}{\tilde{N}} j, \ m, j = 1, \ldots, \tilde{N}, \ k = 1, 2.$$

Tables below show the error E_{L_2} for the two test surfaces, different equation parameter values s and space discretization parameter N.

Table 3. Discrete L_2 error for the case $D = D_1$.

N	Nodes	$s_1 = 1$	$s_2 = 0.5 - 3i$	$s_3 = 2 + 5i$
4	32	4.35e-06	2.41e-06	5.43e-08
8	128	6.12e-07	3.51e-07	3.26e-09
16	512	2.56e-09	6.80e-10	2.27e-11
32	2048	7.32e-12	3.66e-12	4.24e-12

Table 4. Discrete L_2 error for the case $D = D_2$.

N	Nodes	$s_1 = 1$	$s_2 = 0.5 - 3i$	$s_3 = 2 + 5i$
4	32	3.75e-06	8.92e-08	1.37e-08
8	128	4.74e-07	1.27e-08	2.43e-09
16	512	6.31e-09	5.83e-09	1.29e-10
32	2048	7.14e-11	4.29e-11	3.92e-11

The obtained results support error rates, provided by Wienert [15].

4.3. Non-Stationary Problem

In this subsection we test the numerical solution of the non-stationary problem (1)–(3). The first example shows a case with an exactly known solution. The second example shows a case where exact solution is not known, but the boundary condition (3) has a Laplace transform available in closed form. For all examples, as suggested in section 2, we solve only $N_t + 1$ stationary problems to provide approximate values $U_{j,N}(x)$ for the numerical inversion of the Laplace transform. We also apply parameters (α, λ) selection technique, described in section 2 and tested in subsection 4.1.

4.3.1. Example with an Exactly Known Solution

As a sample boundary condition (20) we will choose narrowing of the fundamental solution (4.1) onto Γ_1

$$f(x,t) = \tilde{G}(x, y^*, t), \ x \in \Gamma_1, \ y^* \notin D_1.$$

In this case the exact solution of the problem (1) - (3) is

$$u^*(x,t) = \tilde{G}(x, y^*, t), \quad x \in D_1, \ y^* \notin D_1.$$

Let $y^* = (0, 0, 5)$, $x_0 = (0.1, 0.1, 0.2)$. Table 5 shows the absolute error $E_{abs}^{(t)} = |u^*(x_0, t) - u_{N_t,N}(x_0, t)|$ of the approximate solution $u_{N_t,N}(x,t)$ for the different values of t and discretization parameters N_t, N.

Table 5. Absolute error $E_{abs}^{(t)}$, $\Gamma = \Gamma_1$.

N_t	N	$t = 2$	$t = 2.2$	$t = 2.5$
2	4	2.136812e-05	2.462481e-05	2.837609e-05
	8	1.946759e-06	2.188658e-06	2.331827e-06
	16	2.325619e-08	2.773015e-10	9.600292e-08
	32	1.540043e-08	8.910118e-09	8.651947e-08
4	4	2.137816e-05	2.461644e-05	2.844138e-05
	8	1.962045e-06	2.179749e-06	2.418113e-06
	16	7.838391e-09	8.531891e-09	9.433593e-09
	32	1.884036e-11	5.333509e-11	1.013018e-10
8	4	2.137815e-05	2.461638e-05	2.844134e-05
	8	1.962032e-06	2.179657e-06	2.418072e-06
	16	7.851940e-09	8.624379e-09	9.475018e-09
	32	5.286807e-12	8.816986e-12	1.190821e-11

To verify that obtained error rates agree with error rates of numerical Laplace inversion and stationary problems solution, next table highlights decimal exponents of absolute errors for the same point $x_0 = (0.1, 0.1, 0.2)$ and $t = 2$.

Table 6. Error rates comparison.

Laplace Inversion		Stationary		Non-Stationary	
N_t	$log_{10}(E_{abs})$	N	$log_{10}(E_{abs})$	N_t, N	$log_{10}(E_{abs})$
2	-8	16	-10	2, 16	-8
4	-11	32	-12	4, 32	-11
8	-15	32	-12	8, 32	-12

It is easy to see full discretization of the non-stationary problem results in error rate, defined by the worse error of Laplace inversion and stationary problem solution, which is expected. It also indicates a balanced selection of N_t and N may provide best overall result.

4.3.2. Example Without Exactly Known Solution

Let us consider numerical solution of the non-stationary problem (1)–(3) with the following boundary condition

$$g(x,t) = t^2 e^{-t}, \quad (x,t) \in \Gamma_1 \times (0,\infty). \tag{37}$$

For the stationary problems boundary condition we will use closed form of the Laplace transform of $g(x,t)$

$$G_s(x) = \mathcal{L}_t(f(x,t)) = \frac{2}{(s+1)^3}, \ x \in \Gamma_1, \ s \in \mathbb{C}, s \neq -1.$$

Table 7 shows values of the approximate solution of (1)–(3) for different combinations of N_t, N, different points $x \in D_1$ and time points t.

Table 7. Approximate solution for different N_t, N, x, t.

t	N_t	N	$x = (0.1, 0.05, 0.05)$	$x = (0, 0, 0.4)$
1	2	4	0.35246148	0.35659063
	4	8	0.35245882	0.35987086
	4	16	0.35246211	0.35987241
	4	32	0.35246211	0.35987241
3	2	4	0.45384016	0.44480551
	4	8	0.45327121	0.45057778
	4	16	0.45327211	0.45057821
	4	32	0.45327211	0.45057821
5	2	4	0.17317714	0.16828926
	4	8	0.17226425	0.17033565
	4	16	0.17225089	0.17032869
	4	32	0.17225089	0.17032869

For each combination of x, t we observe increasing number of same decimal digits as N_t, N grow.

Let us consider region D_1 with scaling parameter of the boundary Γ_1 set to $A_1 = 6$. We will calculate and plot numerical solution of the non-stationary problem (1)–(3) with the boundary condition (37) over time interval $t \in (0; 10]$ in two points $x_1 = (0, 0, 0)$ and $x_2 = (2.5, 0, 0)$. Note, two test points are intentionally selected so x_1 is placed "deeper" within the region and point x_2 is closer to the boundary. Parameter A_1 is intentionally selected to significantly scale up the region in order to observe time delay in propagation of the boundary condition behaviour inside the region. To produce the plots, we have chosen time step $\Delta t = 0.2$ and numerically solved problem (1)–(3) 50 times for each test point using discretization parameters $N_t = 4, N = 8$. The entire computation process fits into 2-3 minutes using an average-level PC. This and previous numerical examples were performed using MATLAB.

As can be seen from the Figure 5, the peak value at x_1 is observed at a later time point compared to the peak at x_2, which agrees with the expected behaviour.
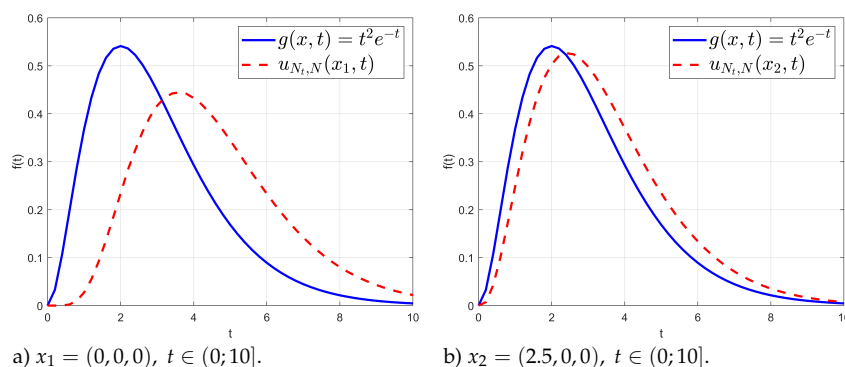
a) $x_1 = (0, 0, 0)$, $t \in (0; 10]$.   b) $x_2 = (2.5, 0, 0)$, $t \in (0; 10]$.

Figure 5. Numerical solution and boundary condition.

5. Conclusions

In this article, an effective combination of the Laplace transform and boundary integral equation method for the numerical solution of 3D initial boundary value problem for the heat equation was proposed and tested. Using observed and proven symmetry in the set of boundary value problems, computation work is reduced by almost a factor of 2. Additional optimization of the integration contour parameters was shown to further reduce the error. As mentioned in the article, due to the independence of the boudanry value problems, the proposed approach is also suitable for parallel computing.

In future work, the presented approach is planned to be tested with other methods for solving boundary value problems, as well as different equations or types of boundary conditions. Additionaly, further research of the optimization techniques for the numerical Laplace transform inversion is planned.

References

1. Kress, R. *Linear Integral Equations*, 3rd ed.; Springer: New York, 2014.
2. Lubich, C.; Schneider, R. Time discretization of parabolic boundary integral equations. *Numerische Mathematik* **1992**, *63*, 455–481.
3. Chapko, R.; Kress, R. Rothe's method for the heat equation and boundary integral equations. *Journal of Integral Equations and Applications* **1997**, *9*, 47–69.
4. Chapko, R.; Kress, R. On the numerical solution of initial boundary value problems by the Laguerre transformation and boundary integral equations. In *Integral and Integrodifferential Equations: Theory, Methods and Applications*; Agarwal, R.; O'Regan, D., Eds.; Gordon and Breach Science Publishers: Amsterdam, 2000; Vol. 2, *Series in Mathematical Analysis and Applications*, pp. 55–69.
5. Chapko, R.; Johansson, B. Numerical solution of the Dirichlet initial boundary value problem for the heat equation in exterior 3-dimensional domains using integral equations. *Journal of Engineering Mathematics* **2017**, *103*, 23–37.
6. Chapko, R.; Johansson, B. A boundary integral equation method for numerical solution of parabolic and hyperbolic Cauchy problems. *Applied Numerical Mathematics* **2018**, *129*, 104–119.
7. Chapko, R.; Mindrinos, L. On the numerical solution of the exterior elastodynamic problem by a boundary integral equation method. *Journal of Integral Equations and Applications* **2018**, *30*, 521–542.
8. Hohage, T.; Sayas, F.J. Numerical solution of a heat diffusion problem by boundary elements methods using the Laplace transform. *Numerische Mathematik* **2005**, *102*, 67–92.
9. Cohen, A.M. *Numerical Methods for Laplace Transform Inversion*; Vol. 5, *Numerical Methods and Algorithms*, Springer: New York, 2007. https://doi.org/10.1007/978-0-387-48987-7.

10.   López-Fernández, M.; Palencia, C. On the numerical inversion of the Laplace transform of certain holomorphic mappings. *Applied Numerical Mathematics* **2004**, *51*, 289–303.

11.   Dingfelder, B.; Weideman, J.A.C. An improved Talbot method for numerical Laplace transform inversion. *Numerical Algorithms* **2015**, *68*, 167–183.

12.   Weideman, J.A.C.; Fornberg, B. Fully numerical Laplace transform methods. *Numerical Algorithms* **2023**, *92*, 985–1006. https://doi.org/10.1007/s11075-022-01368-x.

13.   Gustavsen, B.; Semlyen, A. Rational Approximation of Frequency Domain Responses by Vector Fitting. *IEEE Transactions on Power Delivery* **1999**, *14*, 1052–1061. https://doi.org/10.1109/61.772353.

14.   Andersson, F. Algorithms for Unequally Spaced Fast Laplace Transforms. In Proceedings of the Proceedings of the Project Review, Geo-Mathematical Imaging Group (Purdue University, West Lafayette IN), 2013, Vol. 1, pp. 37–46.

15.   Wienert, L. Die numerische Approximation von Randintegraloperatoren für die Helmholtzgleichung im $\mathbb{R}^3$. PhD thesis, University of Göttingen, 1990.

16.   Colton, D.; Kress, R. *Integral Equation Methods in Scattering Theory*; John Wiley & Sons: New York, 1983; pp. XII + 271.

17.   Abramowitz, M.; Stegun, I. *Handbook of Mathematical Functions with Formulas, Graphs, and Mathematical Tables*; National Bureau of Standards Applied Mathematics Series, Washington, D. C., 1972.